Journal Name

ARTICLE

Boosting Efficiency of Inverted Quantum Dot Light-Emitting Diodes by Balancing Charge Densities and Suppressing Exciton Quenching Through Band Alignment

Received 00th January 20xx,
Accepted 00th January 20xx

DOI: 10.1039/x0xx00000x

www.rsc.org/

Jiangyong Pan, [a,b,†] Changting Wei, [c,†] Lixi Wang, [a,b] Jinyong Zhuang, [c] Qianqian Huang, [a,b] Wenming Su, [c,*] Zheng Cui, [c] Arokia Nathan, [d] Wei Lei, [a,b,*] Jing Chen [a,b,*]

We report an inverted and multilayer quantum dot light emitting diode (QLED) which boosts high efficiency by tuning energy band alignment between charge transport and light emitting layers. The electron transport layer (ETL) was ZnO nanoparticles (NPs) with optimized doping concentration of cesium azide (CsN_3) to effectively reduce electron flow and balance charge injection. This is by virtue of a 0.27 eV upshift of the ETL's conduction band edge, which inhibits the quenching of excitons and preserves superior emissive properties of the quantum dots due to the insulating characteristic of CsN_3. The demonstrated QLED exhibits a peak current efficiency, power efficiency and external quantum efficiency of up to 13.5 cd/A, 10.6 lm/W and 13.4 % for the red QLED, and correspondingly 43.1 cd/A, 33.6 lm/W and 9.1 % for green, and 4.1 cd/A, 2.0 lm/W and 6.6 % for the blue counterparts. Compared with QLEDs without optimization, the performance of these modified devices yield drastic improvement by 95.6%, 39.4% and 36.7%, respectively. The novel device architecture with heterogeneous energy levels reported here, offers a new design strategy for next-generation high efficiency QLED display and solid-state lighting technologies.

Introduction

Since the first report of the colloidal quantum dot light emitting diode (QLED),[1] the device has attracted much attention due to its superior properties over other large-area LED technologies, which include tunable colors, saturated color emission, high luminescence quantum yield, and narrow emission with small full width at half maximum (FWHM).[2-6] These attractive characteristics make the QLED a promising candidate for next generation displays and solid-state lighting.

Over two decades of development, QLED structures has been designed using a variety of materials, that range from inorganic oxides to conjugated polymers and small molecules, as charge-transport interlayers.[7] Previous reported work has focused on the standard QLEDs structure,[8-12] whose external quantum efficiency (EQE) over the years has increased from less than 0.01% to over 20%. The maximum EQE values for R, G, B have been reported to reach up to 20.5%, 14.5%, 15.6%, respectively.[13-16] For example, red QLEDs with EQE over 20% has been reported, which is the highest achieved hitherto thus providing the QLED with strong commercialization potential.[14] Recently, All-inorganic cesium lead halide perovskite ($CsPbX_3$, X = Cl, Br, and I) quantum dots (QDs), possessing high photoluminescence quantum yields and tunable color output, have recently been endowed great promise for high-performance light-emitting diodes (LEDs).[17-20]

In contrast, the inverted architecture is more practical for display applications since it can be easily integrated with a low-cost metal-oxide or silicon thin-film transistor (TFT) technologies.[21] In a typical inverted device structure, the ITO is utilized as the transparent cathode and ZnO nanoparticles (NPs) as the ETL spin-coated on the ITO. This is followed by layer-by-layer deposition of the emissive layer (QDs), hole transport layer (HTL) and anode.[21] In contrast to the conventional QLED structure, electrons and holes in the inverted QLED are injected from ITO and Al, and transported to QDs through the ZnO nanoparticle film (ETL) and organic molecules (HTL), respectively, followed by recombination in the QDs layer. Compared with the standard device architecture, the inverted device structure is superior from the standpoint of processing, because: (i) only the ETL (ZnO NP) and QD emissive layers are deposited by solution processing avoiding organic solvents from undermining the integrity of the underlying layers, (ii) multilayer HTLs with high hole mobility along with the anode can be thermally evaporated continuously without any damage or solvent penetration to the underlying layer (thus accelerating the hole transfer rate

[a.] School of Electronic Science and Engineering, Southeast University, Nanjing, China, 210096,.
[b.] Joint International Research Laboratory of Information Display and Visualization, Southeast University, Nanjing, 210096, China
[c.] Printable Electronics Research Centre, Suzhou Institute of Nano-Tech and Nano-Bionics (SINANO), Chinese Academy of Sciences, Suzhou 215123, China
[d.] Electrical Engineering Division, Engineering Department, University of Cambridge, 9 JJ Thomson Avenue, CB3 0FA, Cambridge,United Kingdom

Electronic Supplementary Information (ESI) available: UPS spectrum of QD film,optical and electronic properties of ZnO NPs, XPS spectrum and absorption spectra of ZnO:CsN_3 film, and the reproducibility test of devices.

and improving QLED performance), (iii) the metal oxide ETL layer can be optimized precisely to reduce the electron flow while enhancing that of holes thereby balancing the carrier transport within the QLED.[22] Recently, a high-performance inverted hybrid structure red QLED with an EQE of 18% was reported.[23] The efficiency (~6.6 cd/A) has also been improved due to the effective capture of electron leakage by phosphorescent molecules and the non-radiative transfer of harvested energy to adjacent QDs.[24] Of equal significance is the turn on voltage which has decreased to 2.04 V due to the reduced hole-injection barrier from the HTL to the QD emitting layer. This serves to improve the injection balance of carriers into the QD layer.[25] In spite of these improvements in device performance, the charge balance in the QD layer is still a key bottleneck that limits the performance.[21, 26-27] A large hole injection barrier exists between the HTL and QD emissive layer due to the shallow level of the highest occupied molecular orbital (HOMO) of the organic layer. In contrast, efficient electron injection is achieved for the ZnO NP as ETL.[28] The methods adopted in many literatures improve the performance of inverted QLED mostly by virtue of facilitating the hole transport.[21, 29-30] As an alternative approach, we can decrease the electron injection from the ETL to balance electron-hole recombination within the emissive layer. The impact of this on QLED performance constitutes the focus of this investigation.

To reduce electron injection, we report results of doping the ZnO ETL with an insulating material of cesium azide (CsN_3) so as to reduce the electron injection. Actually in OLED-related studies, the alkali metals or alkali sub-oxides films such as LiF, Cs_2CO_3, CsF, and CsN_3 can be considered to be used, because they can act as the n-type dopants in contact with emission layer (EML) or ETL, which induces a larger energy bending to modulate the electron injection from cathode to EML.[31-34] In addition, by virture of design and utilization of multilayer HTLs, the charge balance in the device can be optimized, and the superior emissive properties of the QDs can be preserved. It is noted that some conventional solution processed HTL materials, such as PVK and Ploy-TPD are not used here, because it can easily cause the damage or solvent penetration to the underlying layer when the HTL is spin-coated on the QD layer. This strategy offers versatile fabrication of high performance inverted QLEDs with energy band alignments designed to realize a peak current efficiency of up to 13.5 cd/A, 43.1 cd/A and 4.1 cd/A for red, green and blue QLEDs, respectively. The doping concentration and the mechanism for the performance enhancement is fully investigated in this study.

Results and discussion

The corresponding structure of our inverted QLED comprises of ITO/ZnO:CsN_3 /CdSe/ZnS QDs/Di-[4-(N,N-ditolyl-amino)-phenyl] cyclohexane (TAPC)/ dipyrazino [2,3-f:2',3'-h] quinozaline-2,3,6,7,10,11- hexacarbonitrile (HAT-CN) /MoO_3/Al, as shown in Figure 1a. It can be clearly seen from the cross-sectional SEM image of the device (Figure 1b) that the thickness of ZnO:CsN_3, QDs, TAPC and HAT-CN/MoO_3 can be estimated to be about 32 nm, 30 nm, 25 nm and 20 nm, respectively. Illustrated in Figure 1c are schematic energy levels, in which the QDs have a conduction band minimum (CBM) of ~4.8 eV and valence band maximum (VBM) of ~7.1 eV as deduced from UPS spectra (see Figure S1). In addition, typical green light CdSe/ZnS QDs present no surface defect emission, purely consisting of a band edge emission with a peak wavelength of 527 nm and a bandwidth of 25 nm (Figure 1d). Figure 1e presents transmission electron microscopy (TEM) images of green QDs. The average size of QDs was measured to be ~8 nm with high crystallinity. This is indicated in the high resolution TEM. Moreover the ZnO NP layer has an electron affinity of ~4.2 eV and an ionization potential of ~7.7 eV (Figure S2). This can be utilized as an appropriate ETL not only to facilitate the injection of electrons to the QDs, but also to block hole transport across the QD/ETL

Journal Name

ARTICLE

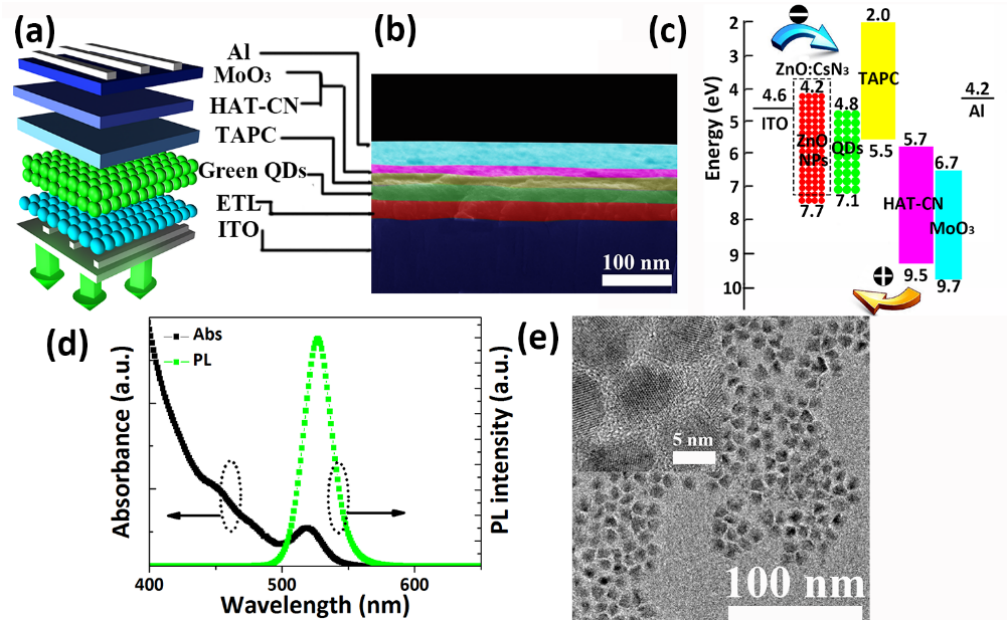

Figure 1. (a) Schematic of the QLED film configuration (b) Cross section SEM of QLED (scale bar, 100 nm) (c) Associated energy level diagram of the QLED. (d) Absorption and PL emission spectra of CdSe/ZnS QDs (e) TEM image of QDs (inset: HRTEM image of QDs)

interface, consequently providing increased exciton recombination efficiency within QD region.[7] Although the electron mobility of ZnO NPs of 1.0×10^{-3} cm^2 V^{-1} s^{-1} (Figure S2) is similar to the hole mobility for the HTL (~1.0×10^{-3} cm^2 V^{-1} s^{-1}),[35-36] hole transport from the HTL to QDs is constrained because of the large energy barrier (>1.6 eV), owing to the shallow lying HOMO level of the TAPC.[37-38] Therefore charge balance can hardly be satisfied in this kind of device structure. This limits the performance of QLED. To address this problem, the insulating material of CsN_3 has been designed and incorporated into the ZnO NPs to decrease the electron injection. A similar strategy has been adopted in the PLEDs with ZnO doped with Cs_2CO_3.[39] It is found that modulation of doping concentration of CsN_3 can obviously impact the overall performance. In this study, the effective doping of CsN_3 into ZnO NPs has been verified from the XPS spectra (Figure S3), which implies the existence of Cs and N elements. In our work, QLEDs were fabricated based on intrinsic films composed of ZnO NPs and CsN_3 with respective (vol%) doping concentrations of 2%, 4 %, 6% and 8%, respectively.

As is well known, the film morphology and roughness are key issues limiting device performance from the standpoint of carrier transport, in particular the leakage current.[22] Herein, the characterization of ZnO:CsN_3 films with the different CsN_3 doping concentration from 0 to 8% (vol%) coated on the ITO were investigated by atom force microscope (AFM) as depicted in Figure 2. The root-mean square (RMS) roughness (Rq) of ZnO film increases significantly from 1.63 nm to 2.45 nm as the doping concentration of CsN_3 increases from 0 to 8 vol%, but the Rq of ZnO NPs film does not change notably if doping ratio of CsN_3 lies within 4 vol%. Therefore we believe that the QLED device utilizing CsN_3 doped ZnO as ETL with a ratio over 4 vol% as ETL does not perform well.

Journal Name

ARTICLE

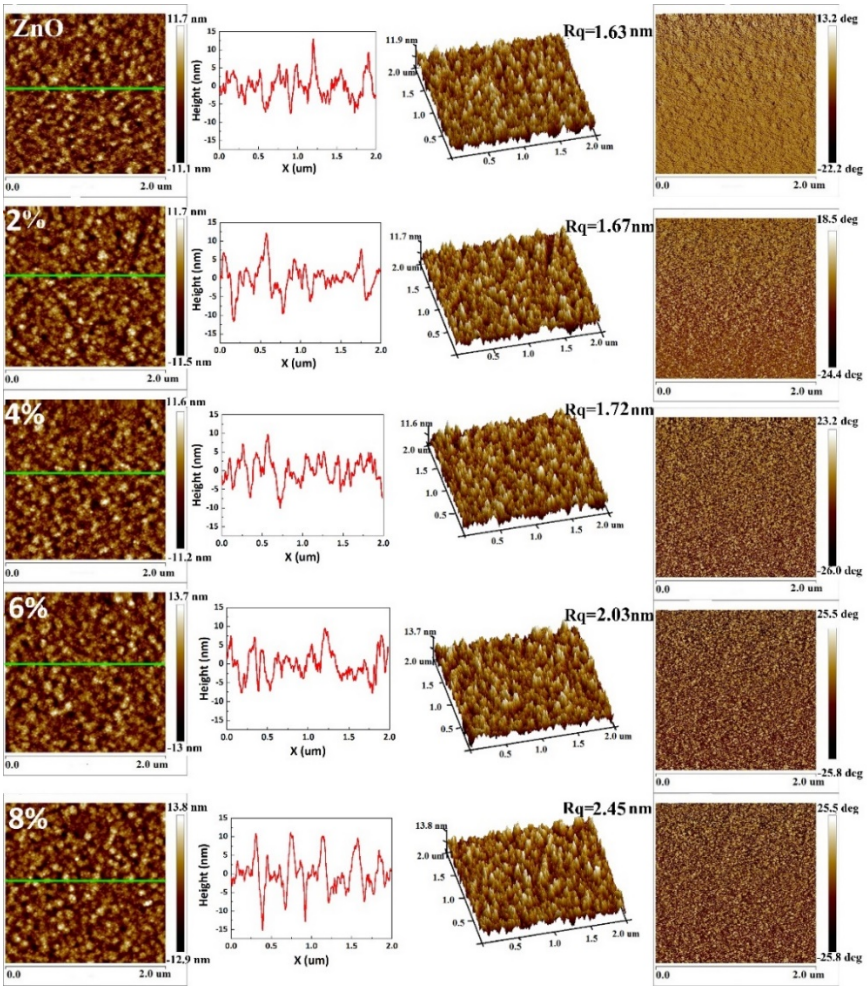

Figure 2. AFM images of the ZnO NPs film at different doping concentration of CsN_3. For each kind of ZnO film, the height, line-scan profile, the pseudo-three-dimensional image and phase images are shown. The surface root-mean square values are displayed in the figure

The electronic structure of the doped ZnO NP films were investigated by ultraviolet photoelectron spectroscopy (UPS) measurements. The resulting secondary-electron cutoff and valence-band regions are shown in Figure 3a and b, respectively. Generally, the work function (WF) could be estimated by the difference between the incident light energy (21.2 eV) and the energy of secondary cutoff. In this case, the WF of ZnO and ZnO:CsN_3(at 4 vol%) are calculated to be 3.96 eV and 3.65 eV, respectively, as labeled in Figure 3a. In order to define the position of the valence band maximum (VBM), the energy gap between Fermi level and VBM (ΔE_{VB}) is extracted from the valence-band region. As shown in Figure 3b, the ΔE_{VB} values of ZnO and ZnO:CsN_3 are 3.71 eV and 3.83 eV, respectively. As a result, via the summation of WF and ΔE_{VB}, the VBM levels of ZnO and ZnO:CsN_3 are calculated to be 7.67 eV and 7.48 eV below the vacuum level, respectively. Figure 3d shows the absorption spectra of ZnO and ZnO:CsN_3, based on data converted from Figure 3c. The band gaps (Eg) of these two materials could be determined through the absorption onset of the linear region and the Eg values for ZnO and ZnO:CsN_3 are found to be 3.46eV and 3.54 eV, respectively. Therefore, the conduction band minimum (CBM) levels are deduced to be 4.21 eV for ZnO and 3.94 eV for ZnO:CsN_3. It is noted that the CBM level of ZnO:CsN_3 is 0.27 eV higher than that of ZnO NPs. Therefore, the transport barrier for electrons from cathode to ETL is larger for ZnO:CsN_3 (0.66 eV) than that for pristine ZnO (0.39 eV), leading to more efficient blocking of electrons and thus balancing carrier injection. In addition, the lowering of CBM of ZnO:CsN_3 helps reduce exciton dissociation, thus reducing the exciton quenching due to the larger energy barrier between the CBM of QDs and ZnO NPs.[40] The specific variation tendency of energy levels for the ZnO with different CsN_3 doping is provided in the Figure S4 to verify the energy level alignment of CsN_3.

Journal Name

ARTICLE

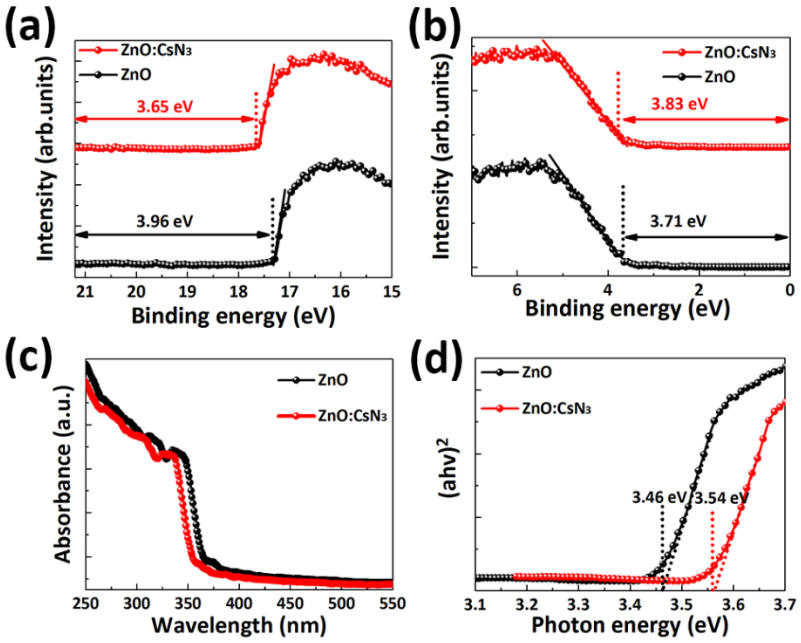

Figure 3. UPS spectra showing (a) high-binding energy secondary electron cutoff and (b) valence-band edge regions of ZnO and ZnO doped CsN_3 films (doping ratio is 4 vol%). (c) Absorption spectra of ZnO, (d) $(Ahv)^2$–hv plots converted from (c).

To study the effect of the doping ratio of CsN_3 on the performance of the device, QLED devices with different CsN_3 doping concentration of ZnO were fabricated and EL characteristics were measured as shown in Figure 4. The current density gradually decreases as the doping concentration of CsN_3 increases as shown in Figure 4a， because the ZnO:CsN_3 tends to block the injection of electrons by virture of its relatively higher CBM as indicated in Figure 3. From Figure 4a, it is apparent that electron injection from the ZnO ETLs to the QDs layers can be modulated and excess electron current in the QLED can be eliminated by adjusting the doping concentration of CsN_3 in ZnO. Similar to the variation tendency of current density, the luminance decreases as doping concentration of CsN_3 increases, but the differences are small if the doping does not exceed 4 vol%. It can be speculated that a doping concentration of 4 vol% yields the highest device efficiency. Correspondingly, the current efficiency (η_A) and power efficiency (η_P) increase from 30.9 cd/A to 43.1 cd/A, and from 23 lm/W to 33.6 lm/W, respectively, yielding enhancement factors of 1.4 compared with the reference device illustrated in Figure 4b. A similar trend is observed for the EQE of the QLED device in Figure 4c whereby the efficiency increases to a maximum of 9.1% at a doping concentration of 4 vol% and then decreases as doping concentration of CsN_3 further increases. It is noted that the devices present good reproducibility (Figure S5). Peak efficiencies of the QLED devices can be achieved at a luminance (L) $\approx 10^3$ cd m^{-2}, and efficiencies close to the peak value (i.e. $\eta_{EQE} \geqslant 85\%$ peak η_{EQE}) are maintained with values ranging from 10^2 to 10^4 cd m^{-2}. These characteristics are highly desirable for displays and lighting applications.[14] For devices with a larger doping ratio of CsN_3 in ZnO, the performance deteriorates. This can be attibuted to the limited carrier injection because of the insulting properties of CsN_3 and the deteriorative smoothness of ETL film, as reflected by the lower injection current. The EL spectra driven at voltages in the range 3 to 6 V is very stable with the same emission peak location as shown in Figure 4d. The result indicates that the exciton recombination zone in QLEDs should not be changed at this operating voltage range. Additionally, it is found that there is no parasitic emission in the EL spectrum, which indicates that the exciton recombination lies completely within the QD layer. Also the location of the EL peak is slightly red-shifted compared with the PL emission peak of QDs measured in octane. This can be attributed to a combination of interdot interactions in closely packed QD solids, and to the electric-field-induced Stark effect.[41-42] Table 1 summarizes the detailed performance parameters for the optimized green QLED.

Journal Name

ARTICLE

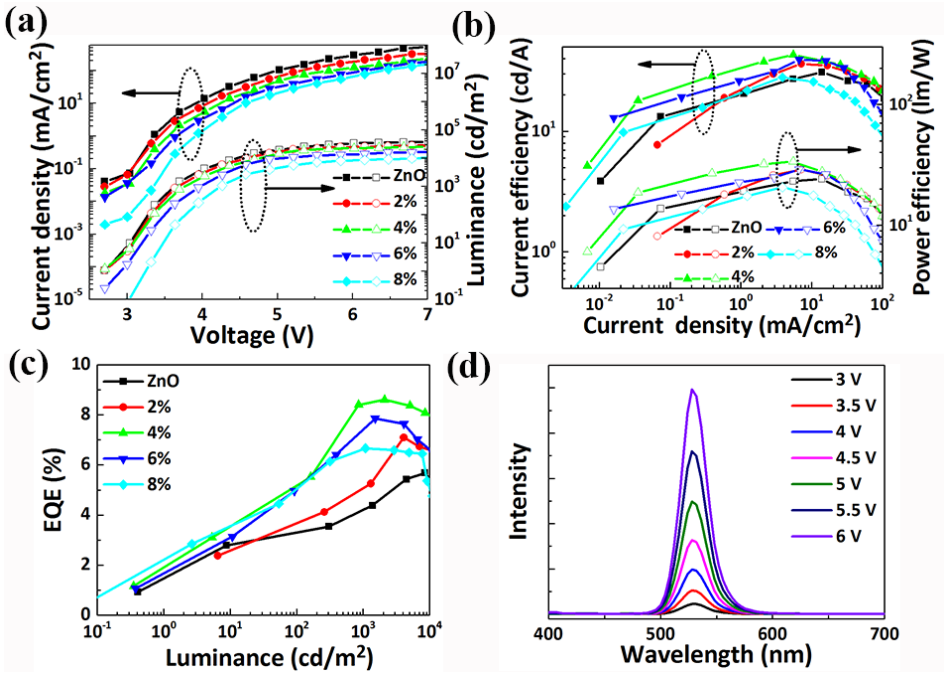

Figure 4. (a) Current density-voltage and luminance-voltage characteristics of the QLED at different doping concentrations of CsN_3 in ZnO, (b) current efficiency and power efficiency and (c) EQE of QLED device at different doping concentrations of CsN_3 in ZnO (d) EL intensity of the QLED under different driving voltages for a CsN_3 doping ratio of 4 vol%

This increase in efficiencies can be attributed to the charge balance, which is caused by the reduction of electron flow. To characterize the electron injection efficiency of the doped ETL, electron-only devices with ITO/ETL/QDs/ZnO/Al at different doping concentration of CsN_3 was fabricated and measured. To determine the optimal doping concentration, hole only devices (ITO/PEDOT/QDs/TAPC/HAT-CN/MoO_3/Al) were also fabricated for comparison as shown in Figure 5. Devices with ZnO:CsN_3 as ETL indeed exhibit remarkably lower electron current than that of devices with ZnO. This is because the position of CBM of ZnO:CsN_3 (3.94 eV) is higher than that of ZnO (4.21 eV) and thus there exists a larger injection barrier (0.66 eV) when electrons are injected from cathode to the ZnO. In addition, the decreased electron current density is due to the increase in internal resistance caused by the insulating property of CsN_3. It turns out that the current density in the electron-only device with doping concentration of 4 vol% becomes similar to that in the hole-only device, indicating a fulfillment of carrier injection balance in the QLED device.

This improvement in efficiencies can also be attributed to the inhibition of exciton quenching as mentioned above. For both photoluminance (PL) and electroluminescence (EL) properties, charging degrades the emissive properties of the quantum dots (QDs)

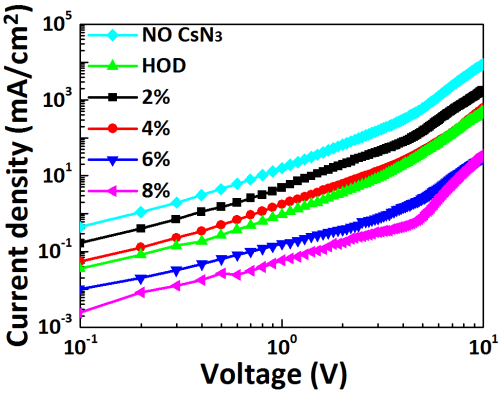

Figure 5. Current density as a function of voltage for the electron-only and hole-only devices.

and causes luminescence quenching.[43-44] The quenching appears to be reduced with doping of CsN_3 in the ETL. To prove the effect of CsN_3 concentration on quenching of excitons, time-resolved photoluminescence (TR-PL) was conducted at a doping concentration of CsN_3 of 4 vol%, which can be fitted well with exponential function (see Table S2).[18] The TR-PL samples were composed of ITO/ZnO: CsN_3 (ETL)/QD (Figure 6a). In this case, when the QDs were in direct contact with the ZnO ETLs, a spontaneous charge transfer process occurs owing to the difference in work functions, leaving positively charged QDs.[23] The charging of the QDs causes inefficient trion emissions,[44] as indicated by the decrease in

the PL lifetime (from 27.8 ns to 14.6 ns, see Table S2) of the QD films when in contact with the underlying ZnO films. It is demonstrated that the exciton quenching can be facilitated by two processes: i) exciton dissociation driven by the large energy-level difference between the conduction band (CB) of QDs and ZnO NPs, and ii) non-radiative energy transfer from QDs to ZnO NPs.[45] The doping of ETL by CsN_3 modifies the QD/ZnO interface, thus increasing the lifetime of the QD film as displayed in the Figure 6a from 14.6 ns to 22.4 ns. This can be attributed to the larger energy barrier (0.86 eV) for exciton dissociation between the CB of QDs and ZnO NPs after doping of CsN_3 in the ZnO as indicated in Figure 3, and the inhibition effect of the insulating layer on exciton quenching induced by ZnO nanoparticles. Thus it appears that the ZnO doped CsN_3 helps maintain charge neutrality of QD emitters thus preserving their superior emissive properties.

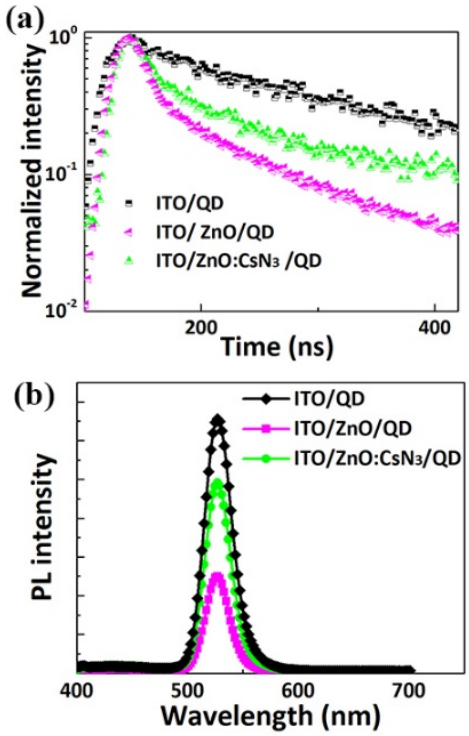

Figure 6. (a) PL lifetime curves of QDs obtained from TR-PL with different ETL and (b) PL intensities of QDs film with different ETLs

To further verify the effect of CsN_3 on blocking of exciton quenching, we conducted steady-state PL with ITO/ETL/QD samples excited using a 360 nm monochromated light source (Figure 6b). After utilizing the ZnO:CsN_3, the PL intensity of QDs increased greatly compared with the QDs utilizing ZnO as ETL. This trend was found to be consistent with the results from TR-PL spectra. Therefore, with a proper doping concentration of CsN_3 in ZnO, we can improve QLED efficiency not only by decreasing electron injection into the QDs to realize charge balance, but also by inhibiting the quenching of excitons.

Following the same design principles, we fabricated red QLEDs with improved performance by optimizing the ETL. As displayed in Figure 7a, the red QDs present a band edge emission with a peak wavelength of 627 nm and a bandwidth of 26 nm. The average size of QDs was measured to be ~10 nm according to TEM depicted in the inset of Figure 7a. The EL characteristics of red QLED based on the ZnO with different doping ratio of CsN_3 were measured as shown in Figure 7b-d. Similar to the variation tendency of green QLED, the current density gradually decreases as the doping concentration of CsN_3 increases as shown in Figure 7b. However the luminance decreases slightly if doping concentration of CsN_3 does not exceed 4 vol%, or it will decreases sharply. Correspondingly, the red QLED based on ZnO:CsN_3 (4%) as ETL shows a maximum η_A, η_P and η_{EQE} of 13.5 cd/A, 10.6 lm/W and 13.4 %, respectively. For comparison, the red QLEDs based on pristine ZnO have a much lower electroluminescence performance (maximum η_A = 6.9 cd /A and η_P = 5.2 lm/W η_{EQE} = 6.5%). As a result, the red QLED based on ZnO:CsN_3 improves by 96.6% from the standpoint of current efficiency. However, it is noted that the turn on voltages of the doped devices are increased, as well as the maximum luminance of the final device decreased a little bit as compared to the non-doped device. This phenomenon mainly originates from the limited electron injection due to the relatively higher CBM of doped ETL as indicated in Figure 3. In addition, it can be partly attributed to the deteriorative smoothness of ETL film, as reflected by the AFM measurement in the Figure 2. Compared with the dramatic improvement in the device efficiency, the slight increase in turn-on voltage has little effect on the overall performance of device.

To achieve blue emission with high electroluminescence efficiency, the structure of QLED was modified. Here, CBP was used as the HTL instead of TAPC to obtain enhanced charge balance and efficiency in the blue devices, considering the deeper VBM of blue QDs. This is displayed in Figure 7e in which the blue QDs present a band edge emission with a peak wavelength of 450 nm and a bandwidth of 22 nm with an average particle size of ~7 nm, as shown in the inset. The EL characteristics of blue QLEDs based on the ZnO with different doping ratio of CsN_3 are shown in Figure 7f-h. It is noted that the optimized doping ratio of CsN_3 for the blue QLED is 6%, which is larger than that of green and red QLEDs. This can be attributed to the deeper position of VBM of the blue QDs, which results in poorer charge imbalance in the blue QLED. Thus, it is necessary to reduce the electron injection further to improve the charge balance. The blue optimized QLED exhibits good electroluminescence performance, with a maximum luminance over 5000 cd m^{-2} and the maximum η_A, η_P and η_{EQE} of 4.1 cd/A, 2.0 lm/W and 6.6%. This is an improvement of 36.7% for the current efficiency compared to that without CsN_3. Moreover, a minor efficiency loss (<20%) was observed when the device brightness was extended to L ≈ 10^2 to 10^4 cd m^{-2}.

Journal Name

ARTICLE

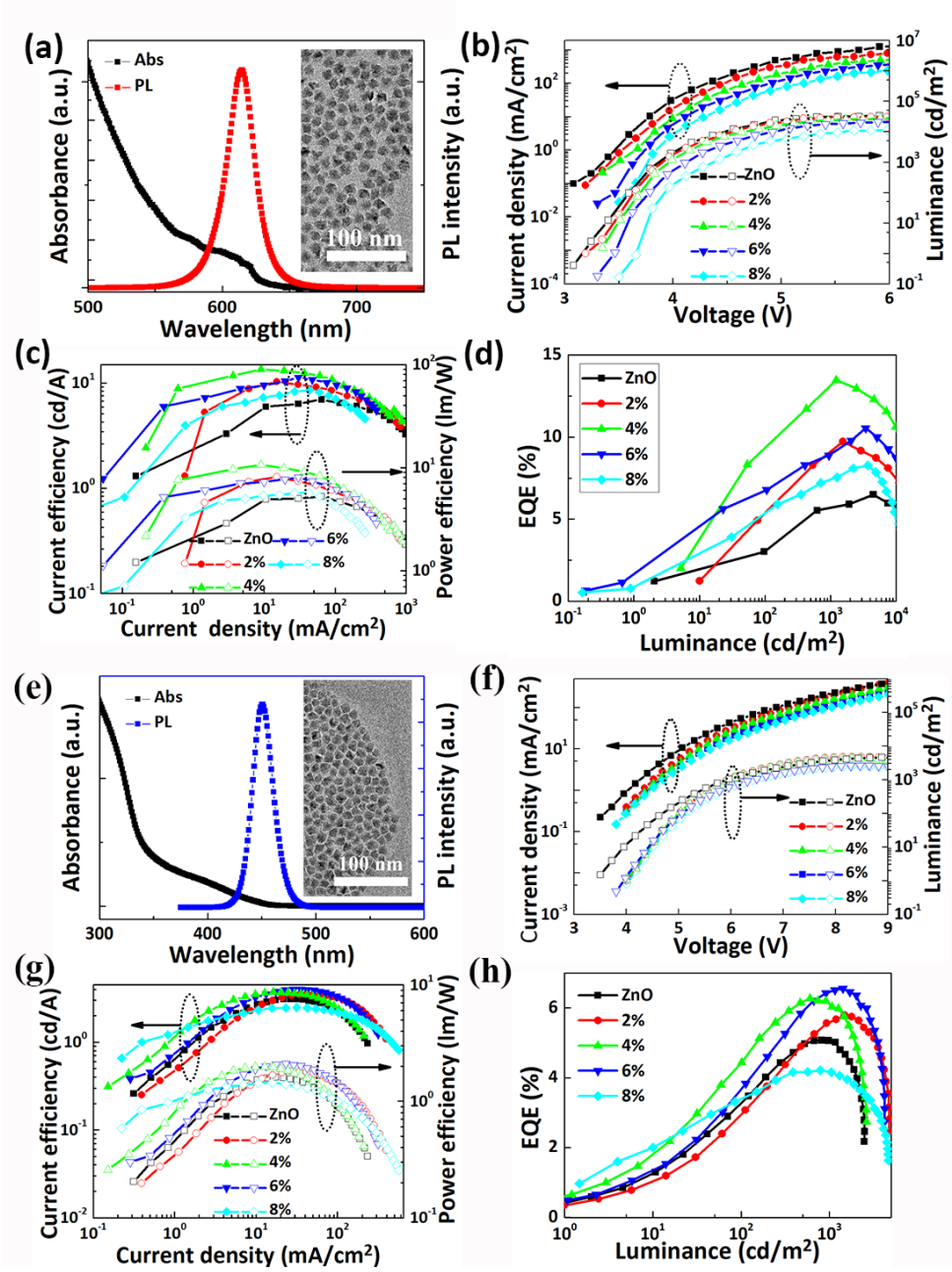

Figure 7. (a)Absorption and PL emission spectra of red QDs. Inset: TEM image of QDs (b) Current density-voltage and luminance- voltage characteristics of the red QLED with different doping concentration of CsN_3 in ZnO . (c) Current efficiency and power efficiency and (d) EQE of red the QLED device at different doping concentrations of CsN_3 in ZnO. (e) Absorption and PL emission spectra of blue QDs. Inset: TEM image of QDs. (f) Current density-voltage and luminance-voltage characteristics of the blue QLED at different doping concentrations of CsN_3 in ZnO. (g) Current efficiency and power efficiency and (h) EQE of the blue QLED device with different doping concentrations of CsN_3 in ZnO

Table 1. Summary of FWHM, turn-on voltage V_T, external quantum efficiency η_{EQE}, power efficiency η_P and current efficiency η_A of optimized green, red and blue QLEDs

Color of QLEDs	FWHM (nm)	V_T (V)	η_{EQE} (%)		η_A (cd/A)		η_P (lm/W)	
			Peak	@ 1000cd m^{-2}	Peak	@ 1000cd m^{-2}	Peak	@ 1000cd m^{-2}
green	26	2.6	9.1	8.5	43.1	38.0	33.6	32.9
red	26	3.0	13.4	13.2	13.5	13.5	10.6	10.3
blue	23	3.3	6.6	6.4	4.1	3.9	2.0	2.0

Figure 8a shows the normalized electroluminescence spectra of blue, green and red QLEDs together with photographs of devices fabricated on 2 cm×2 cm substrates. With emission wavelength peaks at λ = 460 nm, 532 nm and 628 nm, the FWHM is around 23 nm, 26 nm and 26 nm for blue, green and red one, respectively (Table 1). All devices exhibit very saturated and pure colors, as demonstrated by the Commission Internationale de l'Eclairage (CIE) chromaticity diagram shown in Figure 8b. The National Television System Committee (NTSC) standard color triangle is completely covered by the color gamut of the full color QLEDs.

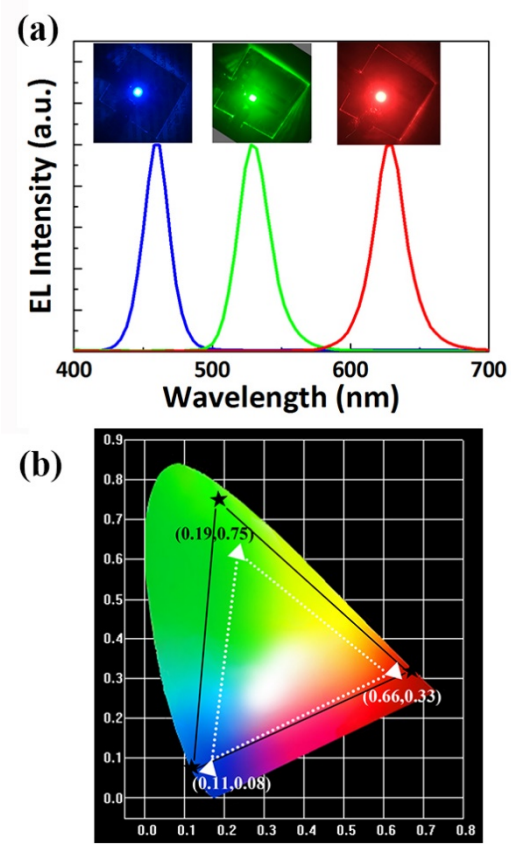

Figure 8. (a) Normalized electroluminescence spectra and images of blue, green and red QLEDs. (b) CIE coordinates of the three color QLEDs (stars) compared to the NTSC color standards (triangles).

Conclusions

The work presented here demonstrates high performance inverted green QLEDs with current efficiency of 43.1 cd/A, power efficiency of 33.6 lm/W and EQE of up to 9.1 %. This was achieved using a conceptually novel structural change in the device by appropriately doping CsN_3 insulator into the ZnO ETL. This not only controls the electron transport flow from electrode to QDs, stemming from the increased energy barrier after CsN_3 doping into ZnO film, but also prevents the exciton quenching at the interface of the ETL/EML as revealed by the TR-PL and PL experiments. A similar device architecture is also adopted for red and blue QLEDs, both of which achieve high performance, i.e.13.5 cd/A, 10.6 lm/W and 13.4 % for the red QLED, 4.1 cd/A, 2.0 lm/W and 6.6 % for the blue QLED. We believe that the approach presented here paves a new design paradigm for carrier balancing so as to boost the performance of inverted QLEDs. The technique shown here has no fundamental obstacles to extend to different colored QLEDs, which would lead to low-cost, high-efficiency, full-color quality electroluminescent devices for both display and solid-state lighting applications.

Experimental

Chemicals. Technical grade oleic acid (OA) (90%), technical grade trioctylphosphine (TOP) (90%), technical grade octadecene (ODE) (90%), CdO (99.5%), Zn acetate (99.99%), S powder (99.998%), and Se powder (99.99%) were obtained from Sigma-Aldrich. ACS grade toluene, 2-ethoxyethanol, methanol and acetone were obtained from Sigma-Aldrich. 1,1-bis[(di-4-tolylamino) phenyl]cyclohexane (TAPC) and dipyrazino [2,3-f:2',3'-h]quinoxaline-2,3,6,7,10,11-hexacarbonitrile (HAT-CN) were purchased from Nichem Fine Technology Co. Ltd. MoO_3 was purchased from Alfa Aesar. All chemicals were used as received.

Synthesis of green QDs Green emitting CdSe/ZnS QDs were synthesized according to a modified method reported previously.[3] Here, 0.4 mmol of CdO, 4 mmol of zinc acetate, 4 mmol of OA, and 20 mL of ODE were mixed in a 100 mL round flask. The mixture was heated to 150 °C degassed under ~10 pa pressure for 30 min, filled with high-purity N_2 flowing, and further heated to 300 °C to form a clear solution of $Cd(OA)_2$ and $Zn(OA)_2$. At this temperature, a stock solution containing 4 mL of TOP, 0.4 mmol of Se, and 4 mmol of S was quickly injected into the reaction flask. After the injection, the reaction temperature was maintained for 10 min to promote the growth of QDs. The reaction was subsequently cooled down to room temperature to stop further growth. The QDs were washed with acetone three times, and finally dispersed in octane at a concentration of 10 mg/mL. The relative ratios of the precursors were varied in order to form QDs with different emissions and

nanostructures. The quantum yield of the red, green and blue QDs is calculated as 85%, 85% and 70%, respectively.

Synthesis of ZnO:CsN_3 ZnO NPs were synthesized as described below. Firstly, zinc acetate, water, and methanol were added to a flask and heated at 60 °C. Then, the potassium hydroxide was dissolved into methanol and added to the flask. The mixture was stirred for 135 mins. The ZnO solution was prepared by dispersing it into 2-ethoxyethanol. The CsN_3 solutions were prepared by dissolving CsN_3 powder into 2-ethoxyethanol with the concentration of 10 mg/mL. Finally, the ZnO:CsN_3 solutions were obtained by blending of ZnO solution and the CsN_3 solutions with different volume ratio.

Device Fabrication All devices were grown on glass substrates precoated with indium tin oxide (ITO) with a sheet resistance of 15 Ω per square. The substrates were cleaned with ultrapurified water and organic solvents and then dry-cleaned for 30 min by exposure to UV–ozone atmosphere. ZnO NPs layer was spin-coated at 2500 rpm onto a UV plasma-treated ITO and then annealed at 120°C for 10 min in the glovebox. After baking the ZnO layer, CdSe/ZnS QDs were spin-coated at 2500 rpm and then heated at 110 °C for 10 min. Subsequently, it was transferred to the thermal evaporation cavity. The TAPC layer acts as the hole transport and electron blocking layer (HTL and EBL), HAT-CN as a HTL and MoO3 as a hole injection layer (HIL) all deposited by thermal evaporation. Then, Al (100 nm) layer was thermally evaporated on top to act as anode. In addition, the thickness of CBP in the blue device is about 30 nm through the surface profile.

Characterization The thickness values of solution-processed films were measured using an AlphaStep profilometer (Veeco, Dektak150). The morphology characterization of the QDs was analyzed using a Cs-corrected high-resolution transmission electron microscope (HRTEM, Tecnai G20). UV-Vis absorption and PL spectra were performed on a Perkin-Elmer Lambda 750 and a Hitachi F460 fluorescence spectrophotometer, respectively. The film surface morphology was measured with Veeco Dimension3100 (USA) at ambient temperature in tapping mode. The work function was measured on the ESCALAB 250 XI X-ray photoelectron spectroscopy at ambient temperature. All electrical testing measurements were performed under ambient conditions without further encapsulation. The electroluminescent spectra were measured with a Spectra Scan PR655. The current-voltage (I–V) and luminance-voltage (L–V) characteristics were measured with a computer controlled Keithley 2400 Sourcemeter. The active area of the device was 2 mm×2 mm, and only the luminance in the forward direction was measured.

Corresponding Author

*E-mail: lw@seu.edu.cn, Phone: +86 25 83792449 Fax: +86 25 833632222; chenjing@seu.edu.cn; wmsu2008@sinano.ac.cn

Author Contributions

The manuscript was written through contributions of all authors. All authors have given approval to the final version of the manuscript.

†These authors contributed equally.

Conflicts of interest

There are no conflicts to declare.

Acknowledgements

This work was supported partially by the National Key R&D Program of China (2016YFB0401600), National Natural Science Foundation Project (61372030, 61571124, and 61674029), Natural Science Foundation Project of Jiangsu Province (BK20151417), and NSFC Research Fund for International Young Scientists(61550110243)， the Scientific Research Foundation of Graduate School of Southeast University YBJJ1714, and the Jiangsu Province College Graduate Research Innovation Program under Grant (KYLX15_0100 and KYLX15_0101)

References

1. Colvin, V. L.; Schlamp, M. C.; Alivisatos, A. P., Light-emitting Diodes Made from Cadmium Selenide Nanocrystals and a Semiconducting Polymer. *Nature* **1994,** *370* (6488), 354-357.

2. Kim, B. H.; Nam, S.; Oh, N.; Cho, S.-Y.; Yu, K. J.; Lee, C. H.; Zhang, J.; Deshpande, K.; Trefonas, P.; Kim, J.-H.; Lee, J.; Shin, J. H.; Yu, Y.; Lim, J. B.; Won, S. M.; Cho, Y. K.; Kim, N. H.; Seo, K. J.; Lee, H.; Kim, T.-i.; Shim, M.; Rogers, J. A., Multilayer Transfer Printing for Pixelated, Multicolor Quantum Dot Light-Emitting Diodes. *ACS Nano* **2016**.

3. Pan, J.; Chen, J.; Huang, Q.; Khan, Q.; Liu, X.; Tao, Z.; Zhang, Z.; Lei, W.; Nathan, A., Size Tunable ZnO Nanoparticles To Enhance Electron Injection in Solution Processed QLEDs. *ACS Photonics* **2016,** *3* (2), 215-222.

4. Pan, J. Y.; Chen, J.; Huang, Q. Q.; Khan, Q.; Liu, X.; Tao, Z.; Lei, W.; Xua, F.; Zhang, Z. C., Flexible Quantum Dot Light Emitting Diodes Based on ZnO Nanoparticles. *RSC Adv.* **2015,** *5* (100), 82192-82198.

5. Pan, J.; Chen, J.; Zhao, D.; Huang, Q.; Khan, Q.; Liu, X.; Tao, Z.; Zhang, Z.; Lei, W., Surface Plasmon-enhanced Quantum Dot Light-emitting Diodes by Incorporating Gold Nanoparticles. *Opt. Express* **2016,** *24* (2), A33-A43.

6. Chang, S.; Zhang, X.; Wang, Z. W.; Han, D. B.; Tang, J. L.; Bai, Z. L.; Zhong, H. Z., Alcohol-Soluble Quantum Dots: Enhanced Solution Processability and Charge Injection for Electroluminescence Devices. *IEEE J. Sel. Top. Quantum Electron.* **2017,** *23* (5), 1900708.

7. Qian, L.; Zheng, Y.; Xue, J. G.; Holloway, P. H., Stable and Efficient Quantum-dot Light-emitting Diodes Based on Solution-processed Multilayer Structures. *Nat. Photonics* **2011,** *5*, 543-548.

8. Daekyoung, K.; Yan, F.; Jungwoo, K.; Ki-heon, L.; Hyoungsub, K.; Heesun, Y.; Heeyeop, C., Improved Electroluminescence of Quantum Dot Light-emitting Diodes Enabled by a Partial Ligand Exchange with Benzenethiol. *Nanotechnol.* **2016,** *27* (24), 245203.

9. Ding, T.; Yang, X.; Ke, L.; Liu, Y.; Tan, W.-Y.; Wang, N.; Zhu, X.-H.; Sun, X. W., Improved Quantum Dot Light-emitting Diodes with a Cathode Interfacial Layer. *Org. Electron.* **2016,** *32*, 89-93.

10. Kim, J.-H.; Han, C.-Y.; Lee, K.-H.; An, K.-S.; Song, W.; Kim, J.; Oh, M. S.; Do, Y. R.; Yang, H., Performance Improvement of Quantum Dot-Light-Emitting Diodes Enabled by an Alloyed ZnMgO Nanoparticle Electron Transport Layer. *Chem. Mater.* **2015,** *27* (1), 197-204.

11. Lee, K.-H.; Han, C.-Y.; Kang, H.-D.; Ko, H.; Lee, C.; Lee, J.; Myoung, N.; Yim, S.-Y.; Yang, H., Highly Efficient, Color-Reproducible Full-Color Electroluminescent Devices Based on Red/Green/Blue Quantum Dot-Mixed Multilayer. *ACS Nano* **2015**.

12. Lee, S. M.; Cho, N.-K.; Kang, S. J., Quantum-dot Light-emitting Diodes with a Double-layer Structured Hole Injection Layer. *J. Vac. Sci. Technol., B* **2015,** *33* (6), 062401.
13. Yang, Y.; Zheng, Y.; Cao, W.; Titov, A.; Hyvonen, J.; MandersJesse, R.; Xue, J.; Holloway, P. H.; Qian, L., High-efficiency Light-emitting Devices based on Quantum Dots with Tailored Nanostructures. *Nat Photon* **2015,** *9*, 259-266.
14. Dai, X.; Zhang, Z.; Jin, Y.; Niu, Y.; Cao, H.; Liang, X.; Chen, L.; Wang, J.; Peng, X., Solution-processed, High-performance Light-emitting Diodes Based on Quantum Dots. *Nature* **2014,** *515*, 96-99.
15. Shen, H.; Cao, W.; Shewmon, N. T.; Yang, C.; Li, L. S.; Xue, J., High-Efficiency, Low Turn-on Voltage Blue-Violet Quantum-Dot-Based Light-Emitting Diodes. *Nano Lett.* **2015,** *15* (2), 1211-1216.
16. Shen, H. B.; Lin, Q. L.; Cao, W. R.; Yang, C. C.; Shewmon, N. T.; Wang, H. Z.; Niu, J. Z.; Li, L. S.; Xue, J. G., Efficient and Long-lifetime Full-color Light-emitting Diodes Using High Luminescence Quantum Yield Thick-shell Quantum Dots. *Nanoscale* **2017,** *9* (36), 13583-13591.
17. Song, J.; Li, J.; Li, X.; Xu, L.; Dong, Y.; Zeng, H., Quantum Dot Light-Emitting Diodes Based on Inorganic Perovskite Cesium Lead Halides (CsPbX3). *Adv. Mater.* **2015,** *27* (44), 7162- 7167.
18. Li, J.; Xu, L.; Wang, T.; Song, J.; Chen, J.; Xue, J.; Dong, Y.; Cai, B.; Shan, Q.; Han, B.; Zeng, H., 50-Fold EQE Improvement up to 6.27% of Solution-Processed All-Inorganic Perovskite CsPbBr3 QLEDs via Surface Ligand Density Control. *Adv. Mater.* **2016,** *29* (5), 1603885-1603893.
19. Li, X.; Wu, Y.; Zhang, S.; Cai, B.; Gu, Y.; Song, J.; Zeng, H., CsPbX3 Quantum Dots for Lighting and Displays: Room-Temperature Synthesis, Photoluminescence Superiorities, Underlying Origins and White Light-Emitting Diodes. *Adv. Funct. Mater.* **2016,** *26* (15), 2435- 2445.
20. Zou, S.; Liu, Y.; Li, J.; Liu, C.; Feng, R.; Jiang, F.; Li, Y.; Song, J.; Zeng, H.; Hong, M.; Chen, X., Stabilizing Cesium Lead Halide Perovskite Lattice through Mn(II) Substitution for Air-Stable Light-Emitting Diodes. *J. Am. Chem. Soc.* **2017,** *139* (33), 11443-11450.
21. Kwak, J.; Bae, W. K.; Lee, D.; Park, I.; Lim, J.; Park, M.; Cho, H.; Woo, H.; Yoon, D. Y.; Char, K.; Lee, S.; Lee, C., Bright and Efficient Full-color Colloidal Quantum Dot Light-emitting Diodes Using an Inverted Device Structure. *Nano Lett.* **2012,** *12*, 2362-2366.
22. Castan, A.; Kim, H. M.; Jang, J., All-Solution-Processed Inverted Quantum-Dot Light-Emitting Diodes. *ACS Appl. Mater. Interfaces* **2014,** *6* (4), 2504-2511.
23. Mashford, B. S.; Stevenson, M.; Popovic, Z.; Hamilton, C.; Zhou, Z. Q.; Breen, C.; Steckel, J.; Bulovic, V.; Bawendi, M.; Coe-Sullivan, S.; Kazlas, P. T., High-efficiency Quantum-dot Lght-emitting Devices with Enhanced Charge Injection. *Nat. Photonics* **2013,** *7*, 407-412.
24. Liu, G.; Zhou, X.; Sun, X.; Chen, S., Performance of Inverted Quantum Dot Light-Emitting Diodes Enhanced by Using Phosphorescent Molecules as Exciton Harvesters. *J. Phys. Chem. C* **2016,** *120* (8), 4667-4672.
25. Ji, W.; Lv, Y.; Jing, P.; Zhang, H.; Wang, J.; Zhang, H.; Zhao, J., Highly Efficient and Low Turn-On Voltage Quantum Dot Light-Emitting Diodes by Using a Stepwise Hole-Transport Layer. *ACS Appl. Mater. Interfaces* **2015,** *7* (29), 15955-15960.
26. Qing, L.; Wen-Yu, J.; Jia-Long, Z.; Chong-Xin, S., Ammonia Reduced Graphene Oxides as a Hole Injection Layer for CdSe/CdS/ZnS Quantum Dot Light-emitting Diodes. *Nanotechnol.* **2016,** *27* (32), 325201.
27. Zhu, H.; Shan, C.-X.; Yao, B.; Li, B.-H.; Zhang, J.-Y.; Zhang, Z.-Z.; Zhao, D.-X.; Shen, D.-Z.; Fan, X.-W.; Lu, Y.-M.; Tang, Z.-K., Ultralow-Threshold Laser Realized in Zinc Oxide. *Adv. Mater.* **2009,** - *21* (- 16), - 1617.
28. Kim, H. Y.; Park, Y. J.; Kim, J.; Han, C. J.; Lee, J.; Kim, Y.; Greco, T.; Ippen, C.; Wedel, A.; Ju, B.-K.; Oh, M. S., Transparent InP Quantum Dot Light-Emitting Diodes with ZrO2 Electron Transport Layer and Indium Zinc Oxide Top Electrode. *Adv. Funct. Mater.* **2016**, n/a-n/a.
29. Son, D. I.; Kim, H. H.; Hwang, D. K.; Kwon, S.; Choi, W. K., Inverted CdSe-ZnS Quantum Dots Light-emitting Diode Using Low-work Function Organic Material Polyethylenimine Ethoxylated. *J. Mater. Chem. C* **2014,** *2* (3), 510-514.
30. Zhang, H.; Li, H.; Sun, X.; Chen, S., Inverted Quantum-Dot Light-Emitting Diodes Fabricated by All-Solution Processing. *ACS Appl. Mater. Interfaces* **2016,** *8* (8), 5493-5498.
31. Piromreun, P.; Oh, H.; Shen, Y.; Malliaras, G. G.; Scott, J. C.; Brock, P. J., Role of CsF on electron injection into a conjugated polymer. *Appl. Phys. Lett.* **2000,** *77* (15), 2403-2405.
32. Huang, J.; Xu, Z.; Yang, Y., Low-Work-Function Surface Formed by Solution-Processed and Thermally Deposited Nanoscale Layers of Cesium Carbonate. *Adv. Funct. Mater.* **2007,** *17* (12), 1966- 1973.
33. Yook, K. S.; Jeon, S. O.; Min, S.-Y.; Lee, J. Y.; Yang, H.-J.; Noh, T.; Kang, S.-K.; Lee, T.-W., Highly Efficient p-i-n and Tandem Organic Light-Emitting Devices Using an Air-Stable and Low-Temperature-Evaporable Metal Azide as an n-Dopant. *Adv. Funct. Mater.* **2010,** *20* (11), 1797- 1802.
34. Vu, H. T.; Huang, C. Y.; Chen, C. J.; Chiang, R. K.; Yu, H. C.; Chen, Y. C.; Su, Y. K., Cesium Azide-An Efficient Material for Green Light-Emitting Diodes With Giant Quantum Dots. *IEEE Photonics Technol. Lett.* **2015,** *27* (20), 2123-2126.
35. Ho, M. D.; Kim, D.; Kim, N.; Cho, S. M.; Chae, H., Polymer and Small Molecule Mixture for Organic Hole Transport Layers in Quantum Dot Light-Emitting Diodes. *ACS Appl. Mater. Interfaces* **2013,** *5* (23), 12369-12374.
36. Tao, Y.; Yang, C.; Qin, J., Organic Host Materials for Phosphorescent Organic Light-emitting Diodes. *Chem. Soc. Rev.* **2011,** *40* (5), 2943-2970.
37. Meyer, J.; Khalandovsky, R.; Görrn, P.; Kahn, A., MoO3 Films Spin-Coated from a Nanoparticle Suspension for Efficient Hole-Injection in Organic Electronics. *Adv. Mater.* **2011,** - *23* (- 1), - 73.
38. Murase, S.; Yang, Y., Solution Processed MoO_3 Interfacial Layer for Organic Photovoltaics Prepared by a Facile Synthesis Method. *Adv. Mater.* **2012,** - *24* (- 18), - 2462.
39. Chiba, T.; Pu, Y.-J.; Hirasawa, M.; Masuhara, A.; Sasabe, H.; Kido, J., Solution-Processed Inorganic–Organic Hybrid Electron Injection Layer for Polymer Light-Emitting Devices. *ACS Appl. Mater. Interfaces* **2012,** *4* (11), 6104-6108.
40. Cao, S.; Zheng, J.; Zhao, J.; Yang, Z.; Li, C.; Guan, X.; Yang, W.; Shang, M.; Wu, T., Enhancing the Performance of Quantum Dot Light-Emitting Diodes Using Room-Temperature-Processed Ga-Doped ZnO Nanoparticles as the Electron Transport Layer. *ACS Appl. Mater. Interfaces* **2017**.
41. Caruge, J.-M.; Halpert, J. E.; Bulović, V.; Bawendi, M. G., NiO as an Inorganic Hole-Transporting Layer in Quantum-Dot Light-Emitting Devices. *Nano Lett.* **2006,** *6* (12), 2991-2994.
42. Kagan, C. R.; Murray, C. B.; Bawendi, M. G., Long-range Resonance Transfer of Electronic Excitations in Close-packed CdSe Quantum-dot Solids. *Phys. Rev. B* **1996,** *54* (12), 8633-8643.
43. Bae, W. K.; Park, Y.-S.; Lim, J.; Lee, D.; Padilha, L. A.; McDaniel, H.; Robel, I.; Lee, C.; Pietryga, J. M.; Klimov, V. I., Controlling the Influence of Auger Recombination on the Performance of Quantum-dot Light-emitting Diodes. *Nat. Commun.* **2013,** *4*.
44. JavauxC; MahlerB; DubertretB; ShabaevA; Rodina, A. V.; EfrosAl, L.; Yakovlev, D. R.; LiuF; BayerM; CampsG; BiadalaL; BuilS; QuelinX; Hermier, J. P., Thermal Activation of Non-radiative Auger

Recombination in Charged Colloidal Nanocrystals. *Nat Nano* **2013,** *8* (3), 206-212.
45. Kim, Y.-H.; Cho, H.; Heo, J. H.; Kim, T.-S.; Myoung, N.; Lee, C.-L.; Im, S. H.; Lee, T.-W., Multicolored Organic/Inorganic Hybrid Perovskite Light-Emitting Diodes. *Adv. Mater.* **2015,** - *27* (- 7), - 1254.

